



A Two-Field Finite Element Solver for Poroelasticity on Quadrilateral Meshes

Graham Harper, Jianguo Liu, Simon Tavener, and Zhuoran Wang^(✉)

Colorado State University, Fort Collins, CO 80523, USA
{harper, liu, tavener, wangz}@math.colostate.edu

Abstract. This paper presents a finite element solver for linear poroelasticity problems on quadrilateral meshes based on the displacement-pressure two-field model. This new solver combines the Bernardi-Raugel element for linear elasticity and a weak Galerkin element for Darcy flow through the implicit Euler temporal discretization. The solver does not use any penalty factor and has less degrees of freedom compared to other existing methods. The solver is free of nonphysical pressure oscillations, as demonstrated by numerical experiments on two widely tested benchmarks. Extension to other types of meshes in 2-dim and 3-dim is also discussed.

Keywords: Bernardi-Raugel elements · Locking-free · Poroelasticity Raviart-Thomas spaces · Weak Galerkin (WG)

1 Introduction

Poroelasticity involves fluid flow in porous media that are elastic and can deform due to fluid pressure. Poroelasticity problems exist widely in the real world, e.g., drug delivery, food processing, petroleum reservoirs, and tissue engineering [6, 7, 19] and have been attracting attention from the scientific computing community [10, 16, 17, 23] (and references therein). Some recent work can be found in [9–11, 20, 24].

Mathematically, poroelasticity can be modeled by coupled Darcy and elasticity equations as shown below

$$\begin{cases} -\nabla \cdot (2\mu\varepsilon(\mathbf{u}) + \lambda(\nabla \cdot \mathbf{u})\mathbf{I}) + \alpha\nabla p = \mathbf{f}, \\ \partial_t(c_0 p + \alpha\nabla \cdot \mathbf{u}) + \nabla \cdot (-\mathbf{K}\nabla p) = s, \end{cases} \quad (1)$$

where \mathbf{u} is the solid displacement, $\varepsilon(\mathbf{u}) = \frac{1}{2}(\nabla\mathbf{u} + (\nabla\mathbf{u})^T)$ is the strain tensor, λ, μ (both positive) are Lamé constants, \mathbf{f} is a body force, p is the fluid pressure,

G. Harper, J. Liu, and Z. Wang were partially supported by US National Science Foundation under grant DMS-1419077.

\mathbf{K} is a permeability tensor (that has absorbed fluid viscosity for notational convenience), s is a fluid source or sink (treated as negative source), α (usually close to 1) is the Biot-Williams constant, $c_0 \geq 0$ is the constrained storage capacity. Appropriate boundary and initial conditions are posed to close the system.

An early complete theory about poroelasticity was formulated in Biot's consolidation model [3]. A more recent rigorous mathematical analysis was presented in [18]. It is difficult to obtain analytical solutions for poroelasticity problems. Therefore, solving poroelasticity problems relies mainly on numerical methods.

According to what variables are being solved, numerical methods for poroelasticity can be categorized as

- *2-field*: Solid displacement, fluid pressure;
- *3-field*: Solid displacement, fluid pressure and velocity;
- *4-field*: Solid displacement and stress, fluid pressure and velocity.

The simplicity of the 2-field approach is always attractive and hence pursued by this paper.

Continuous Galerkin (CG), discontinuous Galerkin (DG), mixed, nonconforming, and weak Galerkin finite element methods all have been applied to poroelasticity problems. A main challenge in all these methods is the *poroelasticity locking*, which often appears in two modes [24]: (i) *Nonphysical pressure oscillations* for low permeable or low compressible media [8, 15], (ii) Poisson locking in elasticity.

Based on the displacement-pressure 2-field model, this paper presents a finite element solver for linear poroelasticity on quadrilateral meshes. The rest of this paper is organized as follows. Section 2 discusses discretization of planar linear elasticity by the 1st order Bernardi-Raugel elements on quadrilaterals. Section 3 presents discretization of 2-dim Darcy flow by the novel weak Galerkin finite element methods, in particular, $WG(Q_0, Q_0; RT_{[0]})$ on quadrilateral meshes. In Sect. 4, the above two types of finite elements are combined with the first order implicit Euler temporal discretization to establish a solver for poroelasticity on quadrilateral meshes, which couples the solid displacement and fluid pressure in a monolithic system. Section 5 presents numerical tests for this new solver to demonstrate its efficiency and robustness (locking-free property). Section 6 concludes the paper with some remarks.

2 Discretization of Elasticity by Bernardi-Raugel (BR1) Elements

In this section, we consider linear elasticity in its usual form

$$\begin{cases} -\nabla \cdot \sigma = \mathbf{f}(\mathbf{x}), & \mathbf{x} \in \Omega, \\ \mathbf{u}|_{\Gamma^D} = \mathbf{u}_D, & (-\sigma \mathbf{n})|_{\Gamma^N} = \mathbf{t}_N, \end{cases} \quad (2)$$

where Ω is a 2-dim bounded domain occupied by a homogeneous and isotropic elastic body, \mathbf{f} is a body force, $\mathbf{u}_D, \mathbf{t}_N$ are respectively Dirichlet and Neumann

data, \mathbf{n} is the outward unit normal vector on the domain boundary $\partial\Omega = \Gamma^D \cup \Gamma^N$. As mentioned in Sect. 1, \mathbf{u} is the solid displacement,

$$\varepsilon(\mathbf{u}) = \frac{1}{2} (\nabla\mathbf{u} + (\nabla\mathbf{u})^T) \quad (3)$$

is the strain tensor, and

$$\sigma = 2\mu \varepsilon(\mathbf{u}) + \lambda(\nabla \cdot \mathbf{u})\mathbf{I}, \quad (4)$$

is the Cauchy stress tensor, where \mathbf{I} is the order two identity matrix.

Note that the Lamé constants λ, μ are given by

$$\lambda = \frac{E\nu}{(1+\nu)(1-2\nu)}, \quad \mu = \frac{E}{2(1+\nu)}, \quad (5)$$

where E is the elasticity modulus and ν is Poisson's ratio.

In this section, we discuss discretization of linear elasticity using the first order Bernardi-Raugel elements (BR1) on quadrilateral meshes. The Bernardi-Raugel elements were originally developed for Stokes problems [2]. They can be applied to elasticity problems when combined with the ‘‘reduced integration’’ technique [4, 5, 24]. In this context, it means use of less quadrature points for the integrals involving the divergence term. The BR1 element on a quadrilateral can be viewed as an enrichment of the classical bilinear Q_1^2 element, which suffers Poisson locking when applied directly to elasticity.

Let E be a quadrilateral with vertices $P_i(x_i, y_i)$ ($i = 1, 2, 3, 4$) starting at the lower-left corner and going counterclockwise. Let e_i ($i = 1, 2, 3, 4$) be the edge connecting P_i to P_{i+1} with the modulo convention $P_5 = P_1$. Let \mathbf{n}_i ($i = 1, 2, 3, 4$) be the outward unit normal vector on edge e_i . A bilinear mapping from (\hat{x}, \hat{y}) in the reference element $\hat{E} = [0, 1]^2$ to (x, y) in such a generic quadrilateral is established as follows

$$\begin{cases} x = x_1 + (x_2 - x_1)\hat{x} + (x_4 - x_1)\hat{y} + ((x_1 + x_3) - (x_2 + x_4))\hat{x}\hat{y}, \\ y = y_1 + (y_2 - y_1)\hat{x} + (y_4 - y_1)\hat{y} + ((y_1 + y_3) - (y_2 + y_4))\hat{x}\hat{y}. \end{cases} \quad (6)$$

On the reference element \hat{E} , we have four standard bilinear functions

$$\begin{aligned} \hat{\phi}_4(\hat{x}, \hat{y}) &= (1 - \hat{x})\hat{y}, & \hat{\phi}_3(\hat{x}, \hat{y}) &= \hat{x}\hat{y}, \\ \hat{\phi}_1(\hat{x}, \hat{y}) &= (1 - \hat{x})(1 - \hat{y}), & \hat{\phi}_2(\hat{x}, \hat{y}) &= \hat{x}(1 - \hat{y}). \end{aligned} \quad (7)$$

After the bilinear mapping defined by (6), we obtain four scalar basis functions on E that are usually rational functions of x, y :

$$\phi_i(x, y) = \hat{\phi}_i(\hat{x}, \hat{y}), \quad i = 1, 2, 3, 4. \quad (8)$$

These lead to eight node-based local basis functions for $Q_1(E)^2$:

$$\begin{bmatrix} \phi_1 \\ 0 \end{bmatrix}, \begin{bmatrix} 0 \\ \phi_1 \end{bmatrix}, \begin{bmatrix} \phi_2 \\ 0 \end{bmatrix}, \begin{bmatrix} 0 \\ \phi_2 \end{bmatrix}, \begin{bmatrix} \phi_3 \\ 0 \end{bmatrix}, \begin{bmatrix} 0 \\ \phi_3 \end{bmatrix}, \begin{bmatrix} \phi_4 \\ 0 \end{bmatrix}, \begin{bmatrix} 0 \\ \phi_4 \end{bmatrix}. \quad (9)$$

Furthermore, we define four edge-based scalar functions on \hat{E} :

$$\begin{aligned} \hat{\psi}_1(\hat{x}, \hat{y}) &= (1 - \hat{x})\hat{x}(1 - \hat{y}), & \hat{\psi}_2(\hat{x}, \hat{y}) &= \hat{x}(1 - \hat{y})\hat{y}, \\ \hat{\psi}_3(\hat{x}, \hat{y}) &= (1 - \hat{x})\hat{x}\hat{y}, & \hat{\psi}_4(\hat{x}, \hat{y}) &= (1 - \hat{x})(1 - \hat{y})\hat{y}. \end{aligned} \tag{10}$$

They become univariate quadratic functions on respective edges of \hat{E} . For a generic convex quadrilateral E , we utilize the bilinear mapping to define

$$\psi_i(x, y) = \hat{\psi}_i(\hat{x}, \hat{y}), \quad i = 1, 2, 3, 4. \tag{11}$$

Then we have four edge-based local basis functions, see Fig. 1 (left panel):

$$\mathbf{b}_i(x, y) = \mathbf{n}_i \psi_i(x, y), \quad i = 1, 2, 3, 4. \tag{12}$$

Finally the BR1 element on a quadrilateral is defined as

$$BR1(E) = Q_1(E)^2 + \text{Span}(\mathbf{b}_1, \mathbf{b}_3, \mathbf{b}_3, \mathbf{b}_4). \tag{13}$$

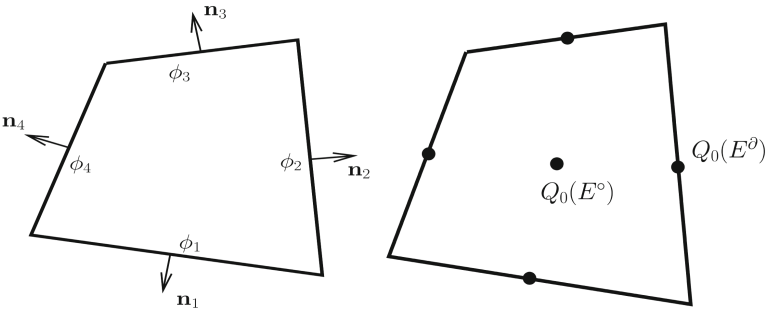


Fig. 1. *Left panel:* Four edge bubble functions needed for the 1st order Bernardi-Raugel element on a quadrilateral; *Right panel:* $WG(Q_0, Q_0; RT_{[0]})$ element on a quadrilateral.

On each quadrilateral, there are totally twelve vector-valued basis functions. Their classical gradients are calculated *ad hoc* and so are the strains. Clearly, their classical divergences are not constants. The elementwise averages of divergence or the local projections into the space of constants are calculated accordingly.

Let \mathbf{V}_h be the space of vector-valued shape functions constructed from the BR1 elements on a shape-regular quadrilateral mesh \mathcal{E}_h . Let \mathbf{V}_h^0 be the subspace of \mathbf{V}_h consisting of shape functions that vanish on Γ^D . Let $\mathbf{u}_h \in \mathbf{V}_h$ and $\mathbf{v} \in \mathbf{V}_h^0$. Then the bilinear form in the strain-div formulation utilizing the Bernardi-Raugel elements reads as

$$\mathcal{A}_h^{SD}(\mathbf{u}_h, \mathbf{v}) = \sum_{E \in \mathcal{E}_h} 2\mu \left(\varepsilon(\mathbf{u}_h), \varepsilon(\mathbf{v}) \right)_E + \lambda (\overline{\nabla \cdot \mathbf{u}_h}, \overline{\nabla \cdot \mathbf{v}})_E, \tag{14}$$

where the overline bar indicates the elementwise averages of divergence. The linear form for discretization of the body force is simply

$$\mathcal{F}_h(\mathbf{v}) = \sum_{E \in \mathcal{E}_h} (\mathbf{f}, \mathbf{v})_E, \quad \forall \mathbf{v} \in \mathbf{V}_h^0. \quad (15)$$

Now there are two sets of basis functions: node-based and edge-based. Compatibility among these two types of functions needs to be maintained in enforcement or incorporation of boundary conditions.

- (i) For a Dirichlet edge, one can directly enforce the Dirichlet condition at the two end nodes and set the coefficient of the edge bubble function to zero;
- (ii) For a Neumann edge, integrals of the Neumann data against the three basis functions (two linear polynomials for the end nodes, one quadratic for the edge) are computed and assembled accordingly.

3 Discretization of Darcy Flow by $\text{WG}(\mathbf{Q}_0, \mathbf{Q}_0; \text{RT}_{[0]})$ Elements

In this section, we consider a 2-dim Darcy flow problem prototyped as

$$\begin{cases} \nabla \cdot (-\mathbf{K}\nabla p) + cp = f, & \mathbf{x} \in \Omega, \\ p|_{\Gamma^D} = p_D, \quad ((-\mathbf{K}\nabla p) \cdot \mathbf{n})|_{\Gamma^N} = u_N, \end{cases} \quad (16)$$

where Ω is a 2-dim bounded domain, p the unknown pressure, \mathbf{K} a conductivity matrix that is uniformly SPD, c a known function, f a source term, p_D a Dirichlet boundary condition, p_D a Neumann boundary condition, and \mathbf{n} the outward unit normal vector on $\partial\Omega$, which has a nonoverlapping decomposition $\Gamma^D \cup \Gamma^N$.

As an elliptic boundary value problem, (16) can be solved by many types of finite element methods. However, *local mass conservation* and *normal flux continuity* are two most important properties to be respected by finite element solvers for Darcy flow computation. In this regard, continuous Galerkin methods (CG) are usable only after postprocessing. Discontinuous Galerkin methods (DG) are locally conservative by design and gain normal flux continuity after postprocessing. The enhanced Galerkin methods (EG) [21] are also good choices. The mixed finite element methods (MFEM) have both properties by design but result in indefinite discrete linear systems that need specially designed solvers. The recently developed weak Galerkin methods [12, 22], when applied to Darcy flow computation, have very attractive features in this regard: They possess the above two important properties and result in symmetric positive linear systems that are easy to solve [12–14].

The weak Galerkin methods [22] rely on novel concepts to develop finite elements for differential equations. Discrete weak basis functions are used separately in element interiors and on interelement boundaries (or mesh skeleton). Then discrete weak gradients of these basis functions are computed via integration by parts. These discrete weak gradients can be established in certain known spaces,

e.g., the local Raviart-Thomas spaces RT_0 for triangles, the standard $RT_{[0]}$ for rectangles, and the unmapped $RT_{[0]}$ for quadrilaterals [14]. These discrete weak gradients are used to approximate the classical gradient in variational forms.

Recall that for a quadrilateral element E , the local unmapped Raviart-Thomas space has dimension 4 and can be generated by these four basis functions

$$RT_{[0]}(E) = \text{Span}(\mathbf{w}_1, \mathbf{w}_2, \mathbf{w}_3, \mathbf{w}_4), \quad (17)$$

where

$$\mathbf{w}_1 = \begin{bmatrix} 1 \\ 0 \end{bmatrix}, \quad \mathbf{w}_2 = \begin{bmatrix} 0 \\ 1 \end{bmatrix}, \quad \mathbf{w}_3 = \begin{bmatrix} X \\ 0 \end{bmatrix}, \quad \mathbf{w}_4 = \begin{bmatrix} 0 \\ Y \end{bmatrix}, \quad (18)$$

and $X = x - x_c$, $Y = y - y_c$ are the normalized coordinates using the element center (x_c, y_c) .

For a given quadrilateral element E , we consider 5 discrete weak functions ϕ_i ($0 \leq i \leq 4$) as follows:

- ϕ_0 for element interior: It takes value 1 in the interior E° but 0 on the boundary E^∂ ;
- ϕ_i ($1 \leq i \leq 4$) for the four sides respectively: Each takes value 1 on the i -th edge but 0 on all other three edges and in the interior.

Any such function $\phi = \{\phi^\circ, \phi^\partial\}$ has two independent parts: ϕ° is defined in E° , whereas ϕ^∂ is defined on E^∂ . Then its discrete weak gradient $\nabla_{w,d}\phi$ is specified in $RT_{[0]}(E)$ via integration by parts [22] (implementation wise solving a size-4 SPD linear system):

$$\int_E (\nabla_{w,d}\phi) \cdot \mathbf{w} = \int_{E^\partial} \phi^\partial(\mathbf{w} \cdot \mathbf{n}) - \int_{E^\circ} \phi^\circ(\nabla \cdot \mathbf{w}), \quad \forall \mathbf{w} \in RT_{[0]}(E). \quad (19)$$

When a quadrilateral becomes a rectangle $E = [x_1, x_2] \times [y_1, y_2]$, we have

$$\begin{cases} \nabla_{w,d}\phi_0 = 0\mathbf{w}_1 + 0\mathbf{w}_2 + \frac{-12}{(\Delta x)^2}\mathbf{w}_3 + \frac{-12}{(\Delta y)^2}\mathbf{w}_4, \\ \nabla_{w,d}\phi_1 = \frac{-1}{\Delta x}\mathbf{w}_1 + 0\mathbf{w}_2 + \frac{6}{(\Delta x)^2}\mathbf{w}_3 + 0\mathbf{w}_4, \\ \nabla_{w,d}\phi_2 = \frac{1}{\Delta x}\mathbf{w}_1 + 0\mathbf{w}_2 + \frac{6}{(\Delta x)^2}\mathbf{w}_3 + 0\mathbf{w}_4, \\ \nabla_{w,d}\phi_3 = 0\mathbf{w}_1 + \frac{-1}{\Delta y}\mathbf{w}_2 + 0\mathbf{w}_3 + \frac{6}{(\Delta y)^2}\mathbf{w}_4, \\ \nabla_{w,d}\phi_4 = 0\mathbf{w}_1 + \frac{1}{\Delta y}\mathbf{w}_2 + 0\mathbf{w}_3 + \frac{6}{(\Delta y)^2}\mathbf{w}_4, \end{cases} \quad (20)$$

where $\Delta x = x_2 - x_1$, $\Delta y = y_2 - y_1$.

Let \mathcal{E}_h be a shape-regular quadrilateral mesh. Let Γ_h^D be the set of all edges on the Dirichlet boundary Γ^D and Γ_h^N be the set of all edges on the Neumann boundary Γ^N . Let S_h be the space of discrete shape functions on \mathcal{E}_h that are degree 0 polynomials in element interiors and also degree 0 polynomials on edges. Let S_h^0 be the subspace of functions in S_h that vanish on Γ_h^D . For (16), we seek $p_h = \{p_h^\circ, p_h^\partial\} \in S_h$ such that $p_h^\partial|_{\Gamma_h^D} = Q_h^\partial(p_D)$ (the L^2 -projection of Dirichlet boundary data into the space of piecewise constants on Γ_h^D) and

$$\mathcal{A}_h(p_h, q) = \mathcal{F}(q), \quad \forall q = \{q^\circ, q^\partial\} \in S_h^0, \quad (21)$$

where

$$\mathcal{A}_h(p_h, q) = \sum_{E \in \mathcal{E}_h} \int_E \mathbf{K} \nabla_{w,d} p_h \cdot \nabla_{w,d} q + \sum_{E \in \mathcal{E}_h} \int_E c p q \quad (22)$$

and

$$\mathcal{F}(q) = \sum_{E \in \mathcal{E}_h} \int_E f q^\circ - \sum_{\gamma \in \Gamma_h^N} \int_\gamma u_N q^\partial. \quad (23)$$

As investigated in [14], this Darcy solver is easy to implement and results in a symmetric positive-definite system. More importantly, it is locally mass-conservative and produces continuous normal fluxes.

4 Coupling BR1 and WG($Q_0, Q_0; RT_{[0]}$) for Linear Poroelasticity on Quadrilateral Meshes

In this section, the Bernardi-Raugel elements (BR1) and the weak Galerkin WG($Q_0, Q_0; RT_{[0]}$) elements are combined with the implicit Euler temporal discretization to solve linear poroelasticity problems.

Assume a given domain Ω is equipped with a shape-regular quadrilateral mesh \mathcal{E}_h . For a given time period $[0, T]$, let

$$0 = t^{(0)} < t^{(1)} < \dots < t^{(n-1)} < t^{(n)} < \dots < t^{(N)} = T$$

be a temporal partition. Denote $\Delta t_n = t^{(n)} - t^{(n-1)}$ for $n = 1, 2, \dots, N$.

Let \mathbf{V}_h and \mathbf{V}_h^0 be the spaces of vector-valued shape functions constructed in Sect. 2 based on the first order Bernardi-Raugel elements. Let S_h and S_h^0 be the spaces of scalar-valued discrete weak functions constructed in Sect. 3 based on the WG($Q_0, Q_0; RT_{[0]}$) elements. Let $\mathbf{u}_h^{(n)}, \mathbf{u}_h^{(n-1)} \in \mathbf{V}_h$ be approximations to solid displacement at time moments $t^{(n)}$ and $t^{(n-1)}$, respectively. Similarly, let $p_h^{(n)}, p_h^{(n-1)} \in S_h$ be approximations to fluid pressure at time moments $t^{(n)}$ and $t^{(n-1)}$, respectively. Note that the discrete weak trail function has two pieces:

$$p_h^{(n)} = \{p_h^{(n),\circ}, p_h^{(n),\partial}\}, \quad (24)$$

where $p_h^{(n),\circ}$ lives in element interiors and $p_h^{(n),\partial}$ lives on the mesh skeleton.

Applying the implicit Euler discretization, we establish the following time-marching scheme, for any $\mathbf{v} \in \mathbf{V}_h^0$ and any $q \in S_h^0$,

$$\begin{cases} 2\mu \left(\varepsilon(\mathbf{u}_h^{(n)}), \varepsilon(\mathbf{v}) \right) + \lambda \overline{(\nabla \cdot \mathbf{u}_h^{(n)}, \nabla \cdot \mathbf{v})} - \alpha \overline{(p_h^{(n),\circ}, \nabla \cdot \mathbf{v})} = (\mathbf{f}^{(n)}, \mathbf{v}), \\ c_0 \left(p_h^{(n),\circ}, q^\circ \right) + \Delta t_n \left(\mathbf{K} \nabla p_h^{(n)}, \nabla q \right) + \alpha \overline{(\nabla \cdot \mathbf{u}_h^{(n)}, q^\circ)} \\ = c_0 \left(p_h^{(n-1),\circ}, q^\circ \right) + \Delta t_n \left(s^{(n)}, q^\circ \right) + \alpha \overline{(\nabla \cdot \mathbf{u}_h^{(n-1)}, q^\circ)}, \end{cases} \quad (25)$$

for $n = 1, 2, \dots, N$. The above two equations are further augmented with appropriate boundary and initial conditions. This results in a large monolithic system.

This solver has two displacement degrees of freedom (DOFs) per node, one displacement DOF per edge, one pressure DOF per element, one pressure DOF

per edge. Let N_d, N_e, N_g be the numbers of nodes, elements, and edges, respectively, then the total DOFs is

$$2 * N_d + N_e + 2 * N_g, \tag{26}$$

which is less than that for many existing solvers for poroelasticity.

5 Numerical Experiments

In this section, we test this novel 2-field solver on two widely used benchmarks. In these test cases, the permeability is $\mathbf{K} = \kappa \mathbf{I}$, where κ is a piecewise constant over the test domain. Finite element meshes align with the aforementioned pieces. Rectangular meshes (as a special case of quadrilateral meshes) are used in our numerics.

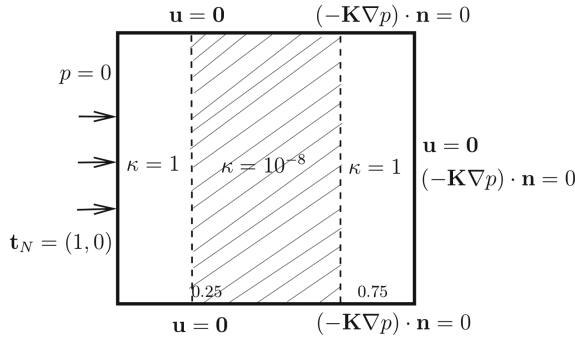


Fig. 2. Example 1: A sandwiched low permeability layer.

Example 1 (A sandwiched low permeability layer). This problem is similar to the one tested in [8,9], the only difference is the orientation. The domain is the unit square $\Omega = (0, 1)^2$, with a low permeability material ($\kappa = 10^{-8}$) in the middle region $\frac{1}{4} \leq x \leq \frac{3}{4}$ being sandwiched by the other material ($\kappa = 1$). Other parameters are $\lambda = 1, \mu = 1, \alpha = 1, c_0 = 0$. Listed below are the boundary conditions.

- For solid displacement:
 - For the left side: Neumann (traction) $-\sigma \mathbf{n} = \mathbf{t}_N = (1, 0)$;
 - For the bottom-, right-, and top-sides: homogeneous Dirichlet (rigid) $\mathbf{u} = \mathbf{0}$;
- For fluid pressure:
 - For the left side: homogeneous Dirichlet (free to drain) $p = 0$;
 - For 3 other sides: homogeneous Neumann (impermeable) $(-\mathbf{K} \nabla p) \cdot \mathbf{n} = 0$.

The initial displacement and pressure are assumed to be zero. See Fig. 2 for an illustration.

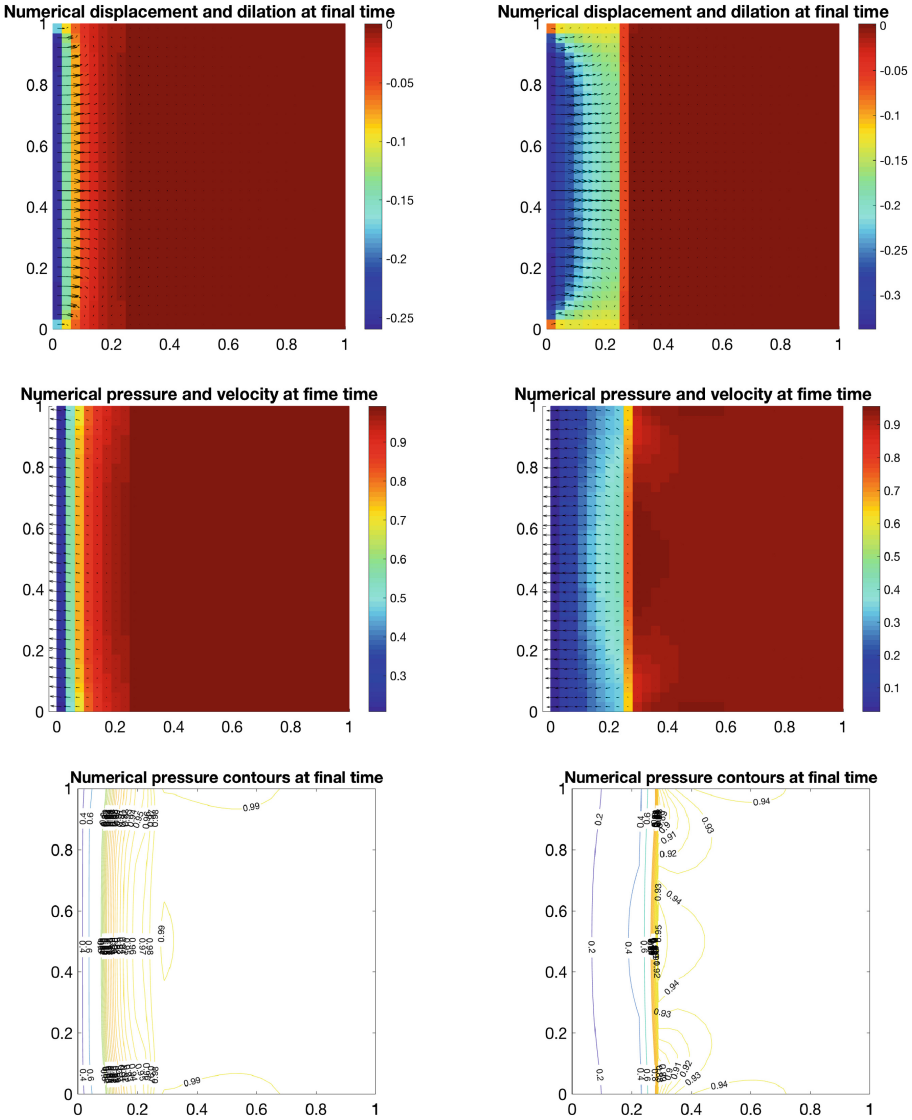


Fig. 3. Sandwiched low permeability layer: Numerical displacement and dilation, numerical pressure and velocity, numerical pressure contours for $h = 1/32$ and $\Delta t = 0.001$. Left column for time $T_1 = 0.001$; Right column for time $T_2 = 0.01$. Further shrinking in solid, drop of maximal fluid pressure, and pressure front moving are observed.

For this problem, we examine more details than what is shown in the literature. We use a uniform rectangular mesh with $h = 1/32$ for spatial discretization and $\Delta t = 0.001$ for temporal discretization. This way, $\Delta t \approx h^2$. Shown in Fig. 3

are the numerical displacement and dilation (div of displacement), the numerical pressure and velocity, and the numerical contours at time $T_1 = 0.001$ and $T_2 = 0.01$, respectively. As the process progresses and the fluid drains out from the left side ($x = 0$), it is clearly observed that

- (i) The maximal pressure is dropped from around 0.9915 to around 0.9570;
- (ii) The pressure front moves to the right and becomes more concentrated around the interface $x = 0.25$;
- (iii) The solid is further shrunk: maximal shrinking (negative dilation) magnitude increases from around 0.2599 to around 0.3385.

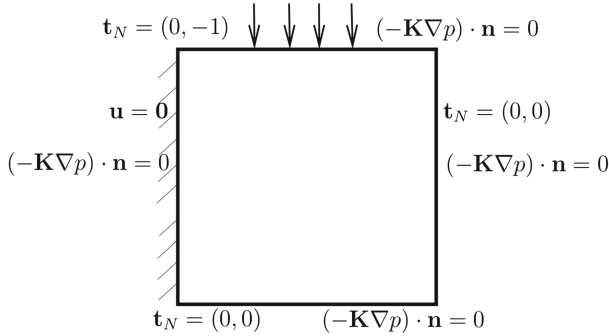


Fig. 4. Example 2: Cantilever bracket problem.

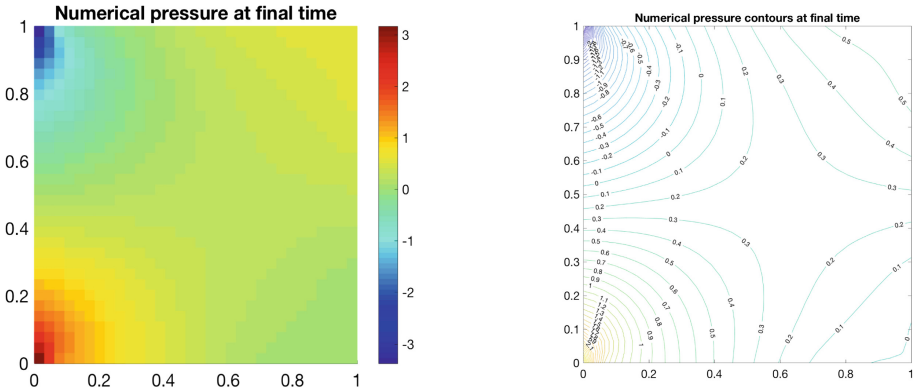


Fig. 5. Example 2: Cantilever bracket problem. Numerical pressure at time $T = 0.005$ is obtained by combining Bernardi-Raugel and weak Galerkin elements through the implicit Euler discretization with $\Delta t = 0.001$, $h = 1/32$.

Example 2 (Cantilever bracket problem). This benchmark is often used to test spurious pressure oscillations [1, 17, 24]. The domain is the unit square $\Omega = (0, 1)^2$. A no-flux (Neumann) condition is prescribed on all four sides for the fluid pressure. The left side is clamped, that is, a homogeneous Dirichlet condition $\mathbf{u} = \mathbf{0}$ is posed for the solid displacement for $x = 0$. A downward traction (Neumann condition) $-\sigma \mathbf{n} = \mathbf{t}_N = (0, -1)$ is posed on the top side, whereas the right and bottom sides are traction-free. The initial displacement and pressure are assumed to be zero. See Fig. 4.

Here we follow [1, 24] to choose the following parameter values

$$E = 10^5, \quad \nu = 0.4, \quad \kappa = 10^{-7}, \quad \alpha = 0.93, \quad c_0 = 0.$$

We set $\Delta t = 0.001$, $h = 1/32$. Shown in Fig. 5 are the numerical pressure profile and contours at $T = 0.005$, obtained from using the Bernardi-Raugel elements and weak Galerkin elements. Clearly, the numerical pressure is quite smooth and there is no nonphysical oscillation.

This new finite element solver has been added to our `Matlab` code package `DarcyLite`. The implementation techniques presented in [13] are used.

It is demonstrated in [24] that nonphysical pressure oscillations occur when the classical continuous Galerkin method is used for elasticity discretization.

6 Concluding Remarks

In this paper, we have developed a finite element solver for linear poroelasticity on quadrilateral meshes based on the two-field model (solid displacement and fluid pressure). This solver relies on the Bernardi-Raugel elements [2] for discretization of the displacement in elasticity and the novel weak Galerkin elements [14] for discretization of pressure in Darcy flow. These spatial discretizations are combined with the backward Euler temporal discretization. The solver does not involve any nonphysical penalty factor. It is efficient, since less unknowns are used, compared to other existing methods. This new solver is robust, free of poroelasticity locking, as demonstrated by experiments on two widely tested benchmarks.

This paper utilizes the unmapped local $RT_{[0]}$ spaces for discrete weak gradients, which are used to approximate the classical gradient in the Darcy equation. Convergence can be established when quadrilateral are asymptotically parallelograms [14]. This type of new solvers are simple for practical use, since any polygonal domain can be partitioned into asymptotically parallelogram quadrilateral meshes. Efficient and robust finite element solvers for Darcy flow and poroelasticity on general convex quadrilateral meshes are currently under our investigation and will be reported in our future work.

Our discussion focuses on quadrilateral meshes, but the ideas apply to other types of meshes. For triangular meshes, one can combine the Bernardi-Raugel elements on triangles for elasticity [2] and the weak Galerkin elements on triangles for Darcy [12]. This combination provides a viable alternative to the

three-field solver investigated in [24]. Similar 2-field solvers can be developed for tetrahedral and cuboidal hexahedral meshes. This is also a part of our current research efforts for developing efficient and accessible computational tools for poroelasticity.

References

1. Berger, L., Bordas, R., Kay, D., Tavener, S.: Stabilized lowest-order finite element approximation for linear three-field poroelasticity. *SIAM J. Sci. Comput.* **37**, A2222–A2245 (2015)
2. Bernardi, C., Raugel, G.: Analysis of some finite elements for the stokes problem. *Math. Comput.* **44**, 71–79 (1985)
3. Biot, M.: General theory of three-dimensional consolidation. *J. Appl. Phys.* **12**, 155–164 (1941)
4. Brenner, S., Sung, L.Y.: Linear finite element methods for planar linear elasticity. *Math. Comput.* **59**, 321–338 (1992)
5. Chen, Z., Jiang, Q., Cui, Y.: Locking-free nonconforming finite elements for planar linear elasticity. In: *Discrete and Continuous Dynamical Systems*, pp. 181–189 (2005)
6. Cheng, A.H.-D.: Poroelasticity. TATPM, vol. 27. Springer, Cham (2016). <https://doi.org/10.1007/978-3-319-25202-5>
7. Cowin, S., Doty, S.: *Tissue Mechanics*. Springer, New York (2007). <https://doi.org/10.1007/978-0-387-49985-7>
8. Haga, J., Osnes, H., Langtangen, H.: On the causes of pressure oscillations in low permeable and low compressible porous media. *Int. J. Numer. Anal. Meth. Geomech.* **36**, 1507–1522 (2012)
9. Hu, X., Mu, L., Ye, X.: Weak Galerkin method for the Biot’s consolidation model. *Comput. Math. Appl.* (2018, in press)
10. Hu, X., Rodrigo, C., Gaspar, F., Zikatanov, L.: A nonconforming finite element method for the Biot’s consolidation model in poroelasticity. *J. Comput. Appl. Math.* **310**, 143–154 (2017)
11. Lee, J., Mardal, K.A., Winther, R.: Parameter-robust discretization and preconditioning of Biot’s consolidation model. *SIAM J. Sci. Comput.* **39**, A1–A24 (2017)
12. Lin, G., Liu, J., Mu, L., Ye, X.: Weak galerkin finite element methdos for Darcy flow: anisotropy and heterogeneity. *J. Comput. Phys.* **276**, 422–437 (2014)
13. Liu, J., Sadre-Marandi, F., Wang, Z.: Darcylite: a matlab toolbox for darcy flow computation. *Proc. Comput. Sci.* **80**, 1301–1312 (2016)
14. Liu, J., Tavener, S., Wang, Z.: The lowest-order weak Galerkin finite element method for the Darcy equation on quadrilateral and hybrid meshes. *J. Comput. Phys.* **359**, 312–330 (2018)
15. Phillips, P.: Finite element methods in linear poroelasticity: theoretical and computational results. Ph.D. thesis, University of Texas at Austin (2005)
16. Phillips, P., Wheeler, M.: A coupling of mixed with discontinuous Galerkin finite element methods for poroelasticity. *Comput. Geosci.* **12**, 417–435 (2008)
17. Phillips, P.J., Wheeler, M.F.: Overcoming the problem of locking in linear elasticity and poroelasticity: an heuristic approach. *Comput. Geosci.* **13**, 5–12 (2009)
18. Showalter, R.: Diffusion in poro-elastic media. *J. Math. Anal. Appl.* **251**, 310–340 (2000)

19. Støverud, K., Darcis, M., Helmig, R., Hassanizadeh, S.M.: Modeling concentration distribution and deformation during convection-enhanced drug delivery into brain tissue. *Transp. Porous Med.* **92**, 119–143 (2012)
20. Sun, M., Rui, H.: A coupling of weak Galerkin and mixed finite element methods for poroelasticity. *Comput. Math. Appl.* **73**, 804–823 (2017)
21. Sun, S., Liu, J.: A locally conservative finite element method based on piecewise constant enrichment of the continuous Galerkin method. *SIAM J. Sci. Comput.* **31**, 2528–2548 (2009)
22. Wang, J., Ye, X.: A weak Galerkin finite element method for second order elliptic problems. *J. Comput. Appl. Math.* **241**, 103–115 (2013)
23. Wheeler, M., Xue, G., Yotov, I.: Coupling multipoint flux mixed finite element methods with continuous Galerkin methods for poroelasticity. *Comput. Geosci.* **18**, 57–75 (2014)
24. Yi, S.Y.: A study of two modes of locking in poroelasticity. *SIAM J. Numer. Anal.* **55**, 1915–1936 (2017)